Writing in turbulent air

Jeroen Bominaar,[1] Mira Pashtrapanska,[1] Thijs Elenbaas,[1] Nico Dam,[1] Hans ter Meulen,[1] and Willem van de Water[2]
[1]*Institute of Molecules and Materials, Applied Molecular Physics, Radboud University, Nijmegen, The Netherlands*
[2]*Physics Department, Eindhoven University of Technology, Postbus 513, 5600 MB Eindhoven, The Netherlands*
(Received 10 July 2007; published 25 April 2008)

We describe a scheme of molecular tagging velocimetry in air in which nitric oxide (NO) molecules are created out of O_2 and N_2 molecules in the focus of a strong laser beam. The NO molecules are visualized a while later by laser-induced fluorescence. The precision of the molecular tagging velocimetry of gas flows is affected by the gradual blurring of the written patterns through molecular diffusion. In the case of turbulent flows, molecular diffusion poses a fundamental limit on the resolution of the smallest scales in the flow. We study the diffusion of written patterns in detail for our tagging scheme which, at short (μs) delay times is slightly anomalous due to local heating by absorption of laser radiation. We show that our experiments agree with a simple convection-diffusion model that allows us to estimate the temperature rise upon writing. Molecular tagging can be a highly nonlinear process, which affects the art of writing. We find that our tagging scheme is (only) quadratic in the intensity of the writing laser.

DOI: 10.1103/PhysRevE.77.046312 PACS number(s): 47.27.Gs, 42.68.Ca, 52.25.Gj

I. INTRODUCTION

In molecular tagging velocimetry, molecules of a fluid or gas are marked and followed in time. Their displacement can be used to infer the fluid velocity. The deformation of written patterns (lines, grids) gives information about the gradients of the velocity field, and the gradual blending of the tagged pattern with the background provides a molecular view on mixing in turbulent flows [1].

To perform molecular tagging velocimetry (MTV) in air and to use it to resolve the small-scale features of turbulence presents a challenge. Such a challenge is worthwhile as a successful application of MTV to turbulent flows would complement existing velocimetry techniques that rely on the scattering of light off added seeding particles. Due to the haphazard emergence of seeding particles in the volume of interest, it is difficult to obtain reliable statistical information about the small-scale turbulent velocity field using these seeding methods. This is especially so if the volume is small. In laser-Doppler velocimetry this problem is known as velocity bias, and it severely affects the measurement of high-order statistics of turbulent flows. Another advantage of molecular tagging is that the deformation of tagged patterns can be studied on the smallest turbulent scales; with seeded particles, this would need a prohibitively large particle density.

Several schemes of molecular tagging velocimetry have been reported, but most have not progressed beyond demonstration of the proof of principle. This is understandable as MTV generally involves highly nontrivial molecular spectroscopy. An exception is the work by Noullez *et al.* who used an MTV technique based on the excited states of the oxygen molecule in a study of fundamental scaling properties of a turbulent air jet [2]. In this paper we will discuss a MTV scheme and demonstrate its use in the case of a fully developed turbulent flow. We will focus on the physical aspects of writing in turbulent air. This concerns the blurring of written patterns both through molecular diffusion and turbulent dispersion and the dependence of the concentration of tagged molecules on the writing laser intensity. It will turn out that those affect the applicability to turbulence measurements in an essential manner.

Let us now briefly and nonexhaustively review existing molecular tagging techniques. In many cases, MTV is a two-step process. After tagging through the creation or dissociation of molecules or by exciting molecules to a long-lived metastable state, the thus written pattern is made visible using laser-induced fluorescence. This is also the basis of the Raman excitation plus laser-induced electronic fluorescence (RELIEF) technique [3] that was used by Noullez *et al.* [2] to measure the statistics of transverse velocity increments in turbulence.

Oxygen molecules in metastable (vibrationally excited) states form the tracers made in the RELIEF method. This method takes advantage of the fact that in homonuclear diatomic molecules transitions between vibrational states are prohibited by the electric-dipole selection rules, so that the excited vibrational states have a relatively long lifetime: a few microseconds in dry atmospheric air. Vibrationally ($\nu''=1$) excited molecular oxygen is created in the focal range of two overlapping laser beams by stimulated Raman scattering. The written patterns are read using a narrow linewidth argon-fluoride (ArF) laser. This laser further excites the vibrationally excited molecules up to the $B(\nu'=7)$ vibronic state of oxygen, and the subsequent fluorescence back to high vibrational levels of the ground electronic state is recorded by an intensified charge-coupled-device (CCD) camera. The problem of the RELIEF technique is the fragility of the excited O_2 molecule, which is easily deexcited as a result of molecular collisions, especially with water molecules.

The tracers in hydroxyl tagging velocimetry are OH radicals [4–7]. In this promising technique photodissociation of water vapor is followed by visualization of the resulting OH radical using laser-induced fluorescence. Since dissociation can be achieved using a single 193-nm photon, the tagging molecule density is linearly dependent on the laser intensity. The write stage is so efficient that the writing laser beam can be split into multiple beams that are crossed to make a grid. Also, the reading step is efficient enough to widen the reading laser beam sufficiently to illuminate this grid.

For phosphorescent tracer molecules the second laser for reading is no longer needed. An example of such a phosphorescent molecule is biacetyl [8,9]. It has a long phosphores-

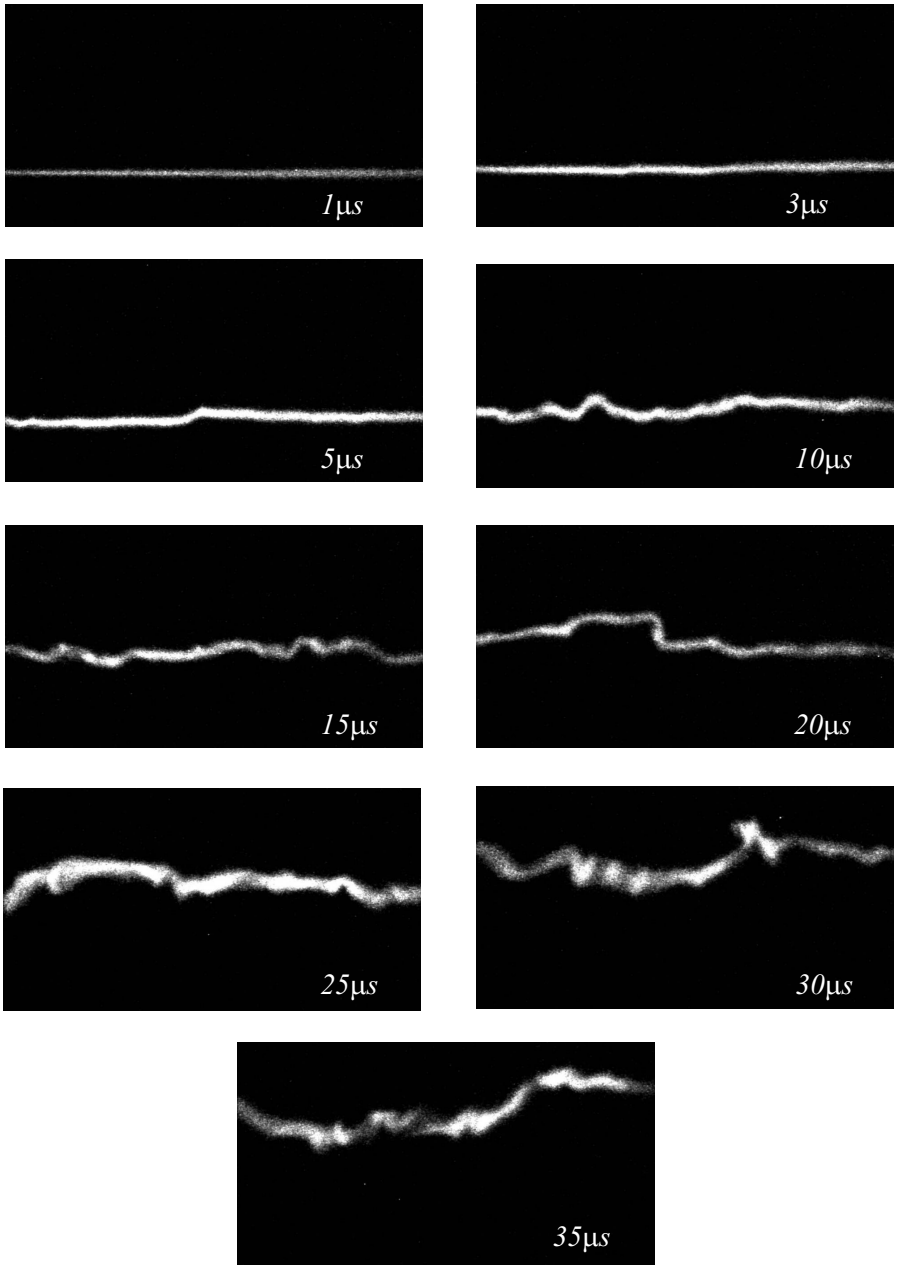

FIG. 1. Lines written in a strongly turbulent jet flow of air (Re_λ=510) using the APART technique. The images shown are registered at the indicated time delays after writing. The lines correspond to different laser shots. Since the laser firing period is two orders of magnitude larger than the large-eddy turnover time, all lines are independent. The horizontal extent of the images is 6.5 mm. The wrinkling of the lines at increasing time delays reflects the action of turbulence. The gradual blurring of the lines is caused by the joint action of molecular diffusion and turbulent dispersion.

cence lifetime (several ms in a N_2 environment) and is efficiently excited. For experiments this means that it is easy to create a multiline grid and consecutive images at several moments in time can be captured using a single laser. The drawbacks are that biacetyl is not a native constituent of air and therefore has to be seeded. Although nontoxic, its smell is severely unpleasant and persistent such that in practice flows can only be measured in a closed circuit. Finally, the lifetime of the phosphorescence is strongly reduced in the presence of molecular oxygen, so that experiments must be performed in an oxygen-free environment.

In this paper we will discuss a scheme for molecular tagging velocimetry which is based on the creation of NO molecules by fusing N_2 and O_2 molecules in plain air in the focus of a strong ultraviolet (uv) laser. A while later these molecules are made visible using laser-induced fluorescence. This technique has been dubbed APART (air photolysis and recombination tracking) [10]. Contrary to the short-lived excited O_2 molecule in the RELIEF technique, the NO molecule is stable. Therefore, this MTV scheme cannot only be used for velocimetry, where the displacement of patterns over short times is studied, but also for studying mixing processes in turbulent flow that stretch over many turnover times of the smallest eddies. Another advantage of this method over the RELIEF technique is that only a single writing laser beam is needed and the delicate overlap of the laser beams required for stimulated Raman scattering is avoided. The success of the technique is illustrated in Fig. 1 which illustrates how lines written in a strongly turbulent flow are deformed as time progresses.

Figure 1 also illustrates a key problem of molecular tagging velocimetry in gases—namely, that written patterns broaden. This leads to a loss of precision of the technique, and it will turn out that this problem is particularly grave for

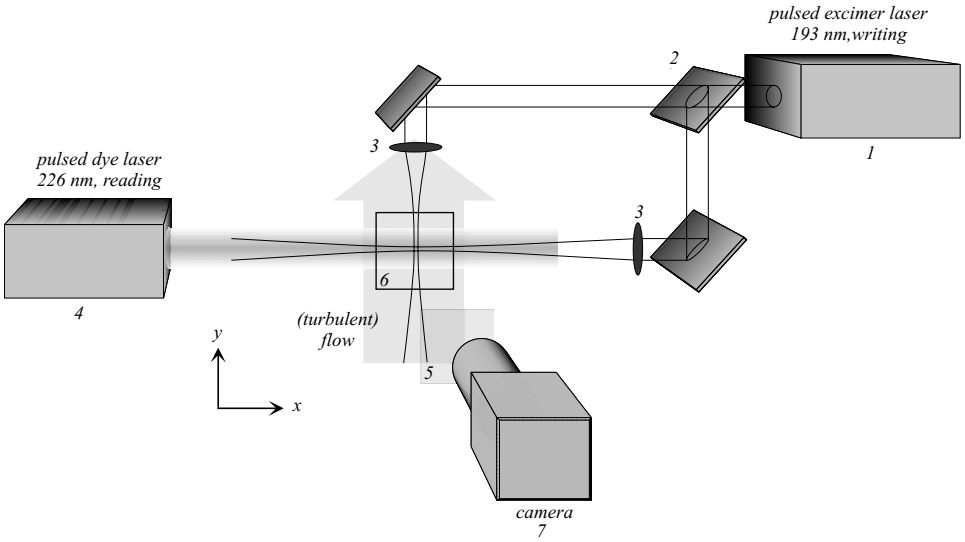

FIG. 2. Experimental setup for molecular tagging. The beam of an ArF excimer laser (1) at $\lambda = 193$ nm is divided into two beams by a beam splitter (2); both are focused into the 6.5×6.5 mm^2 field of view (6) by lenses (3). A while later the created NO molecules are illuminated by a light pulse from the dye laser (4) at $\lambda = 226$ nm. This wavelength is blocked by a dielectric filter (5), which transmits the induced fluorescence. The uv image is registered by a gated, intensified camera (7).

turbulence measurements. A turbulent flow is characterized by a cascade of energy from large to small scales. At the smallest scale, the Kolmogorov scale η, the energy flow balances viscous dissipation. Therefore the size and turnover velocity of the smallest eddies in turbulence are set by viscosity—that is, the diffusion of momentum. On the other hand, the precision of molecular tagging velocimetry is set by the diffusion of mass. Since in a gas momentum diffuses at approximately the same rate as mass, a fundamental limit for the precision of MTV is reached. The purpose of this paper is to explore this fundamental limit and to investigate how it is affected by our specific tagging scheme.

The paper is organized as follows. In Sec. II we will describe the turbulent flow and the optical system used for our molecular tagging experiments. We will briefly describe our procedures to measure the linewidth, but a discussion about how to find severely distorted written lines in a strongly turbulent flow will be published elsewhere [11].

The intrinsic limitation of molecular tagging velocimetry in gases will be discussed in Sec. III. The only cure is to tag heavier molecules which must be seeded in the gas flow. An estimate of how heavy these molecules still may be without compromising their ability to faithfully follow the flow involves the strong intermittency of the local acceleration. Measurements of the spreading rate of lines written in still air are presented in Sec. IV. Since the molecular diffusion coefficient is inversely proportional to pressure, much can be learned from experiments done at increasing pressures.

Much as other optical velocimetry methods in fluid dynamics, MTV is nonintrusive. However, the use of intense laser radiation may in our case lead to local heating due to absorption of radiation. Another source of local heating may be the chemical mechanism that produces the NO molecules. Both processes lead to an increase of the local temperature of the written pattern, which results in an accelerated spreading. In Sec. V we present the results of a simple analytically solvable model that has the initial temperature rise as a free parameter. In this way we arrive at an estimate of the temperature after writing, which is compared to direct measurements of it.

In our molecular tagging scheme the density of tagged molecules depends nonlinearly on the laser intensity. The dependence reflects the response of the excited molecular quantum states that mediate the creation of NO. This nonlinearity can be used in writing: in this way the crossing of two lines would result in a dot. Experiments exploring the nonlinearity are described in Sec. VI.

II. EXPERIMENTAL SETUP

A schematic overview of the experimental setup is given in Fig. 2. Turbulence is measured in the efflux of an axisymmetric jet (not shown). The jet consists of a pressure chamber (typical pressure 1.7 bar) and a 10-cm-diam diffuser that smoothly goes over into a 1-cm-diam orifice. The exit velocity of the air is near sonic (≈ 200 ms^{-1}), which creates a strongly turbulent flow further downstream. The experiments are performed about 40 nozzle diameters downstream (along the y axis) of the orifice where the mean velocity has dropped to $U = 46$ ms^{-1}. For the turbulence experiments in this paper, the turbulent fluctuation velocity is $u = 12.4$ ms^{-1}, the Kolmogorov length $\eta = 14$ μm, the Kolmogorov time $\tau_\eta = 13$ μs, and the Taylor microscale Reynolds number $\mathrm{Re}_\lambda = 510$. The diffusion measurements in stationary gas are done in a pressure cell (not shown), with pressure up until 10 bars. In these measurements also the composition of the gas is varied.

Lines of NO molecules are created through photosynthesis. The beam of a broadband ArF excimer laser (Λ Physik, CompeX 350T) operated at $\lambda = 193$ nm with a pulse energy of about 40 mJ/pulse and a pulse duration of 18 ns is tightly focused in air using a composite lens, specifically optimized for excimer lasers beams, with focal length $f = 250$ mm. A minimum waist diameter of about 50 μm (full width at half maximum) could be made. The resulting Rayleigh range (the distance from the focus where the beam waist has increased from w_0 to $\sqrt{2}w_0$) is approximately 5 mm. The beam waist diameter is about 4 times the Kolmogorov length η. Along this line of focus NO molecules are formed in a process that will be discussed elsewhere [12]. For now, it is important to know that the creation of NO is nonlinearly dependent on laser power. Since the intensity of the writing laser is large enough, more complicated patterns can be written by split-

ting the laser beam, focusing the two resulting beams and crossing them in the field of view.

For reading the written lines, a Nd:YAG pumped dye laser (Spectron or Radiant Dye "Jaguar") is frequency doubled and mixed with the fundamental wavelength of the Nd:YAG laser to obtain radiation with a wavelength of 226 nm. The 226-nm beam is used to excite the $R_{21}(17.5)$ line in the $A \leftarrow X(0,0)$ system (γ bands) of NO and the resulting emission from the A state is detected by a camera system. In the tagging experiments the dye laser beam is aligned anticolinearly to the first excimer beam, perpendicular to the flow direction (see Fig. 2). In some experiments that require a high intensity, the dye laser beam is weakly focused. This is done using a lens with 1000-mm focal length where the focal point is located beyond the readout area. By changing the position of the focus nearer to, or farther from, the readout area, the beam diameter can be regulated to result in maximal intensity while still encompassing the written pattern. In this way the diameter of the beam waist at the camera can be varied between 2 mm and 5 mm. At the largest delay time Δt between reading and writing, $\Delta t = 35$ μs, the rms line displacement is approximately 0.5 mm, which indeed fits inside the beam waist of the reading laser.

An intensified uv-sensitive CCD camera (Photonic Science Coolview) is used to detect the fluorescence from the NO molecules. A custom lens (Bernhard Halle Nachfl.) is used with a fixed focus of 250 mm and $f/2.5$. When the objective and image distances are set for minimal aberrations, a region of 6.5×6.5 mm^2 is imaged onto the intensifier, which is optically linked to the CCD chip. The resolution of the chip in the imaging system is 1024×1024 pixels. The light incident on the camera is filtered using a custom long-pass filter (Laser Optik) with low transmittance (nearly 0%) at 226 nm and high transmittance (>95%) above, thereby effectively removing Rayleigh-scattered light from both lasers while transmitting NO fluorescence. The camera images are captured using a high-speed frame grabber and stored on disk.

The examples of written lines shown in Fig. 1 are obtained under the conditions as described above. Each image was measured using single pulses of both excimer and dye lasers. The spatial resolution of the images is 6.4 μm/pixel. The images show that for short delays, between $\Delta t = 0$ μs and 3 μs the NO production is still in progress and the density (which is proportional to the fluorescence intensity) is not yet maximal. The line intensity finds its maximum between 3 and 5 μs and slowly decreases afterwards. For increasing delay times, turbulence increasingly wrinkles the lines and also redistributes the concentration of markers along the line, even to such an extent that lines can be broken. Finding the centers of such lines is a challenge, which is met by the technique of active contours. Briefly, an active contour in an image is a line, endowed with physical properties (such as elasticity), which is evolved to find a best fit to the corresponding image object. Technically, this is done by turning the image into a potential energy surface with an energy minimum at the sought image object—i.e., the image of the fluorescing NO line [13,14]. Image-processing techniques for MTV will be detailed in a forthcoming publication [11]. Once the line center has been found, the line cross sections are represented by Gaussians $I(z,s) = I_0 + I(s)\exp[-z^2/\sigma(s)^2]$ where z is measured perpendicular to the line center, s is the chord length, and σ is the Gaussian width. The parameters of these Gaussians are determined in a least-squares procedure, assuming that the pixel noise is Poissonian.

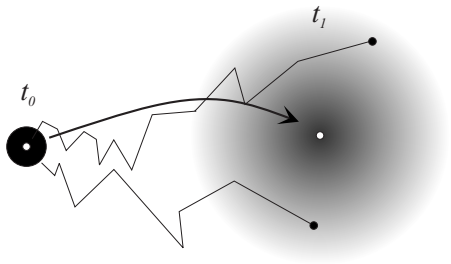

FIG. 3. Molecular tagging velocimetry: the cloud of marked molecules expands during the delay $t_1 - t_0$ between writing and reading. The measured velocity is an average over the molecular trajectories that are determined both by the flow field and the Brownian forces.

III. ROLE OF MOLECULAR DIFFUSION IN MTV

A. Interaction between turbulent flow and diffusion

Naively, one could say that there is nothing which is more appropriate than using the molecules of a fluid for velocimetry. However, it will turn out that a small molecular marker will diffuse at a rate that renders the measurement of small-scale turbulent structures impossible. This is not a contradiction, as there is a clear distinction between molecular motion and the motion of a fluid, a distinction that is rooted in the smallness of the molecular scales in comparison to the scales of the fluid motion.

Fluid flow is the volume-averaged motion of many (Avogadro's number) molecules that at a certain instant reside in a small parcel of fluid. This parcel is so small that the mean motion is independent of its size, but it is also much larger than the mean free path between molecular collisions. In time, marked molecules straggle away from that parcel and move into other parcels, where they will almost instantly adapt to the local mean velocity. The force needed for this adaptation is related to the molecular viscosity.

In tagging velocimetry we infer the velocity from the displacement of the center of mass of a marked cloud of molecules, which is an average over the different fluid velocities that are sampled by the molecules of the spreading cloud. The situation is sketched in Fig. 3. The measured velocity is an average over the molecular trajectories that are determined both by the flow field and the Brownian forces. In tagging velocimetry we infer the (Lagrangian) velocity from the displacement of the center of gravity of clouds of marked molecules between times t_0 and t_1.

Therefore, the interpretation of measured cloud displacements in terms of root-mean-square fluid velocities involves two problems: the underlying Brownian motion of the molecules and the translation of Lagrangian displacements into Eulerian velocities. For times of the order of the small-eddy

turnover time τ_η and clouds with an initial size that is comparable to the Kolmogorov scale η, an approximate expression for the root-mean-square displacement $\langle \Delta^2(t) \rangle$ of the center of mass of a molecular cloud in a time t was derived by Saffman [15], with the result

$$\langle \Delta^2(t) \rangle_f^{1/2} = ut\left(1 - \frac{1}{3} D \frac{\langle \omega^2 \rangle}{u^2} t\right)^{1/2} \approx ut\left(1 - \frac{15^{1/2}}{6} \frac{1}{\mathrm{Sc}} \frac{1}{\mathrm{Re}_\lambda} \frac{t}{\tau_\eta}\right), \tag{1}$$

where Re_λ is the Taylor-based Reynolds number, Sc is the Schmidt number $\mathrm{Sc} = \nu/D$, u is the root-mean-square turbulent velocity with ω its vorticity, and the average $\langle \cdots \rangle_f$ is done over realizations of the turbulent velocity field. The assumption underlying Eq. (1) is that the size of the cloud is so small that different fluid velocities in it are related through the velocity gradient computed in its center of mass.

In the absence of diffusion ($\mathrm{Sc} = \infty$), Eq. (1) expresses that the root-mean-square displacement of the center of mass of a molecular cloud equals $u\ t$. Since the straggling molecules conduct an average over fluid parcels, the apparent rms velocity is reduced. The effect in Eq. (1) is proportional to the ratio of small-scale and large-scale velocities, which at a given τ_η is gauged by the Reynolds number Re_λ. However, it is a small effect; in our experiments, with $\mathrm{Re}_\lambda \approx 500$ and delay times $t/\tau_\eta \approx 3$, the predicted effect is a mere 0.3% reduction of the apparent rms velocity.

While the center-of-mass motion of a cloud is *reduced* by molecular diffusion, its spreading relative to its center of mass is *enhanced* [15]. In other words, there is a *constructive* interference between turbulent and molecular diffusion: the spreading rate of a cloud is more than the sum of both mechanisms separately. This is a subtle effect, since in the Eulerian frame the interference is *destructive*. Moreover, it was recently shown in [16] that the nature of the interference, whether it is constructive or destructive, depends on the detailed behavior of the correlation function of Lagrangian velocities. Interestingly, there should be a rather strong dependence of the interference on the Schmidt number. This dependence will be explored in future experiments.

We have measured the root-mean-square turbulent velocity u from the rms displacement of lines at various time delays. The result is shown in Fig. 4. An average was done over $N = 4 \times 10^3$ lines and over the extent of each line. The statistical error in the measurement of u was estimated by $N^{-1/2}(L_{\mathrm{int}}/L)^{-1/2}u$, where we have assumed Gaussian statistics of the velocity samples and where $L_{\mathrm{int}} = \int_0^\infty \rho(\delta) d\delta$ is the integral over the normalized correlation function

$$\rho(\delta) = [\langle u^2(x+\delta)u^2(x) \rangle - \langle u^2 \rangle^2]/(\langle u^4 \rangle - \langle u^2 \rangle^2),$$

and L is the length of the lines over which u was averaged [17]. Another source of error, which was not considered in the error estimate, is related to finding the backbone of the written lines from the images. The variation of the measured u in Fig. 4 is of the order of the statistical error, and no systematic dependence of u on the delay time is observed. Clearly, in order to see the effect of the lagging molecular cloud, a much better statistical accuracy is needed, with a number of lines that is two orders of magnitude larger. Incidentally, it is remarkable that u can be measured so well from clouds whose size at long times has grown to $\approx 10\eta$.

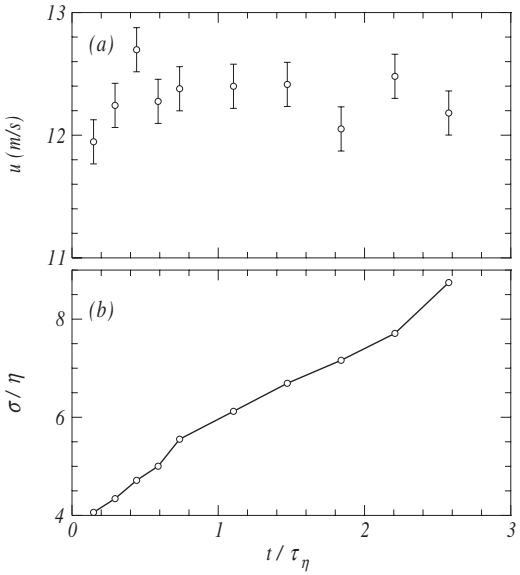

FIG. 4. (a) The root-mean-square velocity u measured from the displacement of lines. The error bars indicate the statistical error of the measurement of u. (b) The Gaussian width σ of tagged lines as a function of the time delay between writing and reading in a strongly turbulent jet flow ($\mathrm{Re}_\lambda = 510$, $\eta = 14\ \mu\mathrm{m}$, $\tau_\eta = 13\ \mu\mathrm{s}$).

B. Sc=1 conundrum

A fundamental problem of molecular tagging velocimetry in turbulent flows of gases is that it can never resolve the smallest turbulent scales, even if written lines are infinitely thin. The reason is that the size of these smallest structures is determined by the diffusion of momentum, while the resolution of our velocimetry method is determined by the diffusion of mass. In gases momentum and mass diffuse at the same rate. Their ratio, the Schmidt number $\mathrm{Sc} = \nu/D$, where D is the mass diffusion coefficient and ν is the kinematic viscosity, is of order 1. The argument can be made quantitative by considering the diffusion of a point cloud in a time equal to the small-eddy turnover time—that is, the Kolmogorov time τ_η. In this time, a fluid parcel will have displaced over the Kolmogorov length η. The size Δ_d of the cloud is then

$$\Delta_d = (4D\tau_\eta)^{1/2} = (4\nu\ \mathrm{Sc}\ \tau_\eta)^{1/2} = [4\nu\ \mathrm{Sc}(\nu/\epsilon)^{1/2}]^{1/2} = 2\eta\ \mathrm{Sc}^{1/2}, \tag{2}$$

where we have used that $\tau_\eta = (\nu/\epsilon)^{1/2}$ and $\eta = (\nu^3/\epsilon)^{1/4}$. Therefore, in a smallest-eddy turnover time a line will always broaden to the Kolmogorov length. Physical lines made of tracer molecules whose mass is comparable to that of the fluid molecules will therefore always iron out the smallest wrinkles of the corresponding mathematical line. Since Δ_d increases with the square root of the delay time t and the displacement is proportional to t, it is of no help to use smaller delay times.

When the molecules of a gas itself are used for tagging in a turbulent flow, written patterns inevitably spread to the size

of the Kolmogorov scale η in a Kolmogorov time τ_η. For velocimetry, τ_η is the typical time between writing and reading. Therefore, even if the written lines are infinitely thin at the instant of writing, they will have broadened to at least η at times of practical interest. The precision of a small-scale velocity measurement is determined by the ratio of the width σ of a line over its small-scale displacement $\Delta_s = v_K t$, with $v_K = (\nu\epsilon)^{1/4}$ the Kolmogorov velocity. With $\sigma(t) = (4Dt)^{1/2}$ we find that

$$\frac{\sigma}{\Delta_s} = 2\mathrm{Sc}^{-1/2}(t/\tau_\eta)^{-1/2}.$$

Although this ratio becomes arbitrarily small at long times, it only does so at times much larger than the small-eddy turnover time, where a velocity can no longer be inferred unambiguously from a measured displacement.

In order to resolve motion on the Kolmogorov scale, we need tracers that have a much larger Schmidt number. At the same time, these tracers must still be small enough so as to be able to follow the largest accelerations of the turbulent velocity field. Since these tracers cannot be the indigenous molecules of the gas, we need to seed the flow with them. We will now derive an expression for the largest size such a tracer may have.

Let us assume that tracer particles are spheres with radius r and mass density ρ_p. The reaction time of these particles to changes of the velocity field is the Stokes time $\tau_S = 2r^2\rho_p/(9\nu\rho_g)$, where ρ_g is the mass density of the gas. The Stokes time must be smaller than the time scale of the velocity field $\tau_f = u/a$, where u and a are the variances of the velocity and acceleration. Taking the dimensional Kolmogorov estimate for the acceleration variance, $\langle a^2 \rangle = a_0 \epsilon^{3/2} \nu^{-1/2}$, we have

$$\tau_f = \tau_\eta \, \mathrm{Re}_\lambda^{1/2} \, 15^{-1/4} a_0^{-1/2}.$$

Using the typical values $\mathrm{Re}_\lambda = 10^3$, $\tau_\eta = 2 \times 10^{-5}$ s, $L = 10^{-2}$ m, $\rho_p = 10^3$, $\rho_g = 1$ kg m^{-3}, and $a_0 = 5$, we find that $\tau_S < \tau_f$ for particles with $r \lesssim 10^{-6}$ m. However, it turns out that the acceleration is an extremely intermittent quantity with highly non-Gaussian probability density functions and the acceleration variance a is a poor measure of the actual accelerations that occur in strongly turbulent flows which can be several orders of magnitude larger than a [18]. Allowing for a factor 10^2, we find $r < 10^{-7}$ m; these particles have a diffusion coefficient $D \approx 10^{-9}$ m^2 s^{-1}, while the diffusion coefficient of NO molecules is $D = 1.8 \times 10^{-5}$ m^2 s^{-1}. We conclude that the choice of tracer molecules is not stringent; in particular, the phosphorescent molecules discussed in the introduction would make tracers that can resolve the smallest scales in turbulence.

IV. DIFFUSION OF LINES

The displacement information of written patterns is filtered through molecular diffusion. This blurring may be accelerated by heat deposited in the writing process. Absorption of radiation leads to a temperature increase, which causes enhanced molecular diffusion and an additional spread through thermal expansion of the tagged cloud. These processes affect in a significant way the application of molecular tagging velocimetry to turbulence. Since the rate of molecular diffusion is inversely proportional to the pressure, key information about line spreading can be learned from measurements at various pressures.

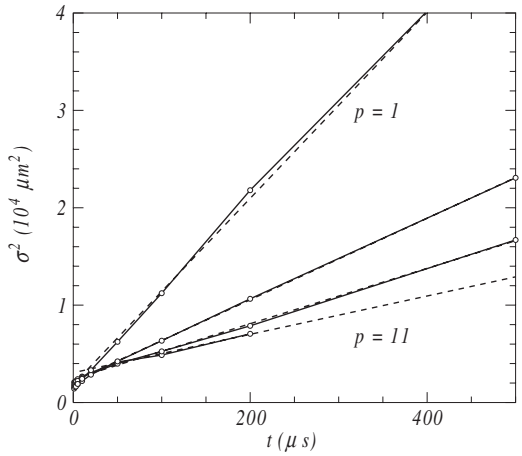

FIG. 5. The increase of the width $\sigma^2(t)$ of lines written in a gas mixture with reduced oxygen content at various pressures: from top to bottom, $p = 1$, 3, 6, and 11 bars, respectively. At the highest pressure ($p = 11$ bars) the spreading rate is smallest and σ^2 is clearly nonlinear. The dashed lines are best linear fits $\sigma^2(t) = A + 4Dt$, from which the diffusion coefficient D shown in Fig. 6 is derived.

Experiments to study the widening of lines were performed both at atmospheric pressure in ambient air and at pressures up to 11 bars in a closed cell. It turned out that the high-pressure experiments had to be done with reduced O_2 content to avoid optical breakdown in the writing laser focus. Two experiments were done, with 0.24% and 0.49% oxygen in N_2, respectively; they produced the same results for the rate of line widening. At each pressure and each time delay between reading and writing, ten lines were written and registered. These images were averaged, and Gaussians, $I(y) = I_0 + I \exp(-y^2/\sigma^2)$, where the line center is assumed at $y = 0$, were fitted to the line cross sections. Since there is no turbulence, all lines run parallel to the x axis (see Fig. 2).

For purely diffusive broadening, the Gaussian width $\sigma(t)$ of a line increases with time t as

$$\sigma^2(t) = \sigma^2(0) + 4Dt. \tag{3}$$

Figure 5 shows $\sigma^2(t)$ measured at pressures ranging from 1 to 11 bars. For low pressures and long delay times, $\sigma(t)$ indeed increases linearly with delay time t. However, at high pressures and short delay times, $\sigma^2(t)$ increases *nonlinearly* with time. This nonlinear part will be explained in Sec. V. From linear fits to the asymptotic (linear) part of the measured spreading $\sigma^2(t)$, we determined the dependence of the (effective) diffusion constant on pressure.

The striking result, shown in Fig. 6 is that the diffusion constant D depends on pressure as

$$D = 0.37 \times 10^{-5} + 2.04 \times 10^{-5} p^{-1}, \tag{4}$$

with the pressure p in bars and D in m^2 s^{-1}. When we ignore the constant offset, this can be compared well to the nominal

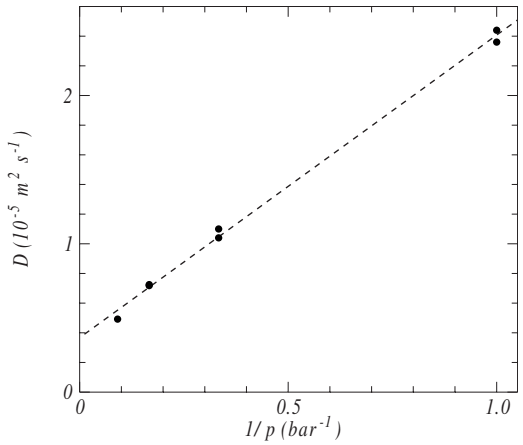

FIG. 6. Dots: the diffusion rate D of written lines as a function of pressure. Dashed line: fit $D=0.37\times10^{-5}+2.04\times10^{-5}p^{-1}$. Because in simple gases the diffusion coefficient is proportional to p^{-1}, we plot the measured D as a function of p^{-1}. The nonvanishing D at $p^{-1}=0$ is due to the heating of the gas in the writing process.

value of the NO diffusion constant in plain air which is $D=1.8\times10^{-5}p^{-1}$. Clearly, the offset must be attributed to heating of the air in the writing process. In the next section we will explain this anomalous spreading with a simple model that assumes a temperature rise of the gas in which lines of NO are written.

V. EFFECT OF HEAT RELEASED IN WRITING

Let us assume that at the instant of writing $t=0$ an amount of heat is deposited in the air, which subsequently spreads through diffusion and convection. It will turn out that the main effect of the temperature rise is convection of the tagged molecules away from the line center. A minor effect is an increase of the molecular diffusion coefficient. The system of equations describing these effects can in one dimension almost miraculously be solved analytically. As the initial temperature rise is a parameter of our model, it can be used to estimate the temperature rise from a measured dispersion curve.

The effect of the temperature rise at $t=0$ is a decrease of the density ρ of the gas, resulting in a convection velocity and an enhanced flow of molecules out of the laser focus. It also affects the values of the mass and heat diffusion coefficients. Finally, the enhanced temperature may also affect the detection of NO fluorescence, which may influence the apparent line profile. Our model does not account for the latter effect.

These processes are gauged by two parameters: namely, the mass diffusion coefficient D and the heat conduction coefficient λ. For convenience we assume that D and the temperature diffusivity $\kappa=\lambda/(\rho c_v)$, where c_v is the specific heat at constant volume, are proportional to the absolute temperature squared T^2, so that $\rho^2 D$ and $\rho^2\kappa$ do not depend on temperature. This assumed temperature dependence, which makes an analytic solution of our model possible, is close to the actual one, $D,\kappa\propto T^{1.7}$.

We assume that at $t=0$ the writing process has established a Gaussian initial temperature and NO concentration profile. We also assume that the air is an ideal gas, with the equation of state

$$p=\rho R_g T, \tag{5}$$

with R_g the gas constant. Then the temperature satisfies

$$\rho c_p\frac{DT}{Dt}-\frac{Dp}{Dt}=\nabla\cdot(\lambda\nabla T), \tag{6}$$

with

$$\frac{D}{Dt}=\left(\frac{\partial}{\partial t}+\boldsymbol{u}\cdot\nabla\right),$$

where $\boldsymbol{u}(x,t)$ is the velocity of the air and c_p is the specific heat at constant pressure. At the time scales of interest we can ignore the dynamics of the pressure, so that we drop the term Dp/Dt [19]. This low-Mach-number approach is rationalized in [20]. For the tagged NO density ρ_t we have the advection diffusion equation

$$\frac{\partial\rho_t}{\partial t}+\nabla\cdot(\rho_t\boldsymbol{u})=-\nabla\cdot\boldsymbol{J}_t, \tag{7}$$

with

$$\boldsymbol{J}_t=-\rho D\nabla(\rho_t/\rho),$$

while the total density ρ of the air satisfies mass balance

$$\frac{\partial\rho}{\partial t}+\nabla\cdot(\rho\boldsymbol{u})=0. \tag{8}$$

The system of equations (5)–(8) signifies the following physics: upon writing, the absorbed heat induces a temperature rise, which results in a lower density [through Eq. (5)], which induces a convection velocity $\boldsymbol{u}$ through Eq. (8), which then enhances the transport of the tagged molecules through Eq. (7). It will appear that this complicated set of partial differential equations can be solved analytically in one dimension. If we introduce the concentration $y_t(x,t)=\rho_t(x,t)/\rho(x,t)$ of tagged molecules, we can summarize them as

$$\rho c_p\left\{\frac{\partial T}{\partial t}+u\frac{\partial T}{\partial x}\right\}=\frac{\partial}{\partial x}\left(\lambda\frac{\partial T}{\partial x}\right),$$

$$\rho\frac{\partial y_t}{\partial t}+\rho u\frac{\partial y_t}{\partial x}=\frac{\partial}{\partial x}\left\{D\rho\frac{\partial y_t}{\partial x}\right\},$$

$$\frac{\partial\rho}{\partial t}+\frac{\partial}{\partial x}(\rho u)=0,$$

$$\rho R_g T=p.$$

Let us now introduce nondimensional variables through

$$\tilde{\rho}=\frac{\rho}{\rho_0},\quad \tilde{T}=\frac{T}{T_0},\quad \tilde{\lambda}=\frac{\lambda}{\lambda_0},\quad \tilde{D}=\frac{D}{D_0},$$

$$\tilde{x} = \frac{x}{R}, \quad \tilde{t} = \frac{t}{\tau_D}, \quad \tilde{u} = \frac{u}{U},$$

with the diffusion time scale $\tau_D = R^2/D_0$, and consequently the velocity scale $U = R/\tau_D$, and where ρ_0, T_0 and D_0 are the values at room temperature and atmospheric pressure ($T_0 = 293$ K, $p_0 = 10^5$ N m^{-2}), and R is the Gaussian width of the initially written line. Omitting the tilde, we can then write

$$\rho\left\{\frac{\partial T}{\partial t} + u\frac{\partial T}{\partial x}\right\} = \frac{1}{\mathrm{Le}}\frac{\partial}{\partial x}\left(\lambda\frac{\partial T}{\partial x}\right), \tag{9}$$

$$\rho\frac{\partial y_t}{\partial t} + \rho u\frac{\partial y_t}{\partial x} = \frac{\partial}{\partial x}\left\{D\rho\frac{\partial y_t}{\partial x}\right\}, \tag{10}$$

$$\frac{\partial \rho}{\partial t} + \frac{\partial}{\partial x}(\rho u) = 0 \tag{11}$$

$$\rho T = 1,$$

with the Lewis number $\mathrm{Le} = D/\kappa$, which we assume to be 1.

Lagrangian coordinates

The convection velocity $u(x,t)$ can be removed from our equations by moving to Lagrangian (or von Mises) coordinates. They are defined by

$$(x,t) \to (\Psi, s),$$

with

$$\Psi = \int_0^x \rho(x',t)dx' \quad \text{and} \quad s = t.$$

Then the material derivative becomes

$$\frac{\partial}{\partial t} + u\frac{\partial}{\partial x} = \frac{\partial}{\partial s} + (\rho u|_{x=0})\frac{\partial}{\partial \Psi} = \frac{\partial}{\partial s},$$

if we take $\rho u|_{x=0} = 0$ at the lower bound of the integral. The inverse transform is

$$x(\Psi, s) = \int_0^\Psi \frac{1}{\rho(\Psi', s)}d\Psi' \quad \text{and} \quad t(\Psi, s) = s.$$

The convection velocity $u(x,t)$ can be recovered from the mass balance equation (11),

$$\frac{\partial \rho}{\partial s} + \rho^2\frac{\partial u}{\partial \Psi} = 0,$$

so that

$$u(\Psi, s) = -\int_0^\Psi \frac{1}{\rho^2(\Psi', s)}\frac{\partial \rho}{\partial s}d\Psi'.$$

As we have argued above, we now make the plausible assumption that for constant pressure the dimensionless heat conductivity and diffusion coefficient are given by

$$\rho\lambda = 1 \quad \text{and} \quad \rho^2 D = 1.$$

It has the pleasant consequence that the diffusive terms on the right-hand side of Eqs. (9) and (10) now have a constant (unit) diffusion coefficient in Lagrangian coordinates,

$$\frac{\partial}{\partial x}\left(\lambda\frac{\partial T}{\partial x}\right) \Rightarrow \rho\frac{\partial^2 T}{\partial \Psi^2}, \tag{12}$$

so that we are left with the equations

$$\frac{\partial T}{\partial s} = \frac{1}{\mathrm{Le}}\frac{\partial^2 T}{\partial \Psi^2},$$

$$\frac{\partial y_t}{\partial s} = \frac{\partial^2 y_t}{\partial \Psi^2},$$

$$\rho T = 1. \tag{13}$$

These equations can be solved analytically using the fundamental solution of the diffusion equation. A solution for the time-dependent density and temperature profile then proceeds as follows: First we assume an initial temperature profile where the temperature in the center of the written line is a factor ΔT above ambient (absolute) temperature:

$$T(x, t=0) = 1 + \Delta T\, e^{-x^2}.$$

This allows us to compute the Lagrangian coordinate Ψ at initial time, $\Psi = \int_0^x T^{-1}(x',0)dx'$, and allows us to express the initial temperature in Lagrangian coordinates, $T(\Psi, 0)$. The temperature now satisfies the ordinary diffusion equation (13), and from the initial temperature profile $T(\Psi, 0)$ we can compute the temperature at later times $T(\Psi, s)$ through the fundamental solution

$$T(\Psi, s) = \frac{1}{(4\pi s)^{1/2}}\int_{-\infty}^{\infty} T(\Psi', 0)e^{-(\Psi - \Psi')^2/4s}d\Psi'. \tag{14}$$

A similar procedure can be followed to compute the time-dependent fraction of tagged molecules $y_t(\Psi, s)$. Finally, we will use Eq. (14) to revert back to physical variables,

$$x = \int_0^\Psi \frac{1}{\rho(\Psi', s)}d\Psi' = \int_0^\Psi T(\Psi', s)d\Psi'.$$

Some of the integrals must be computed numerically, but this effort is negligible compared to the numerical solution of partial differential equations. In the simple numerical scheme that we have used, mass (heat) is conserved to within 5×10^{-3}.

The computed line profile $\rho_t(x,t)$ for scaled initial temperature increase $\Delta T = 2$ and scaled time $t = 1$ is shown in Fig. 7. It is seen that it differs from the Gaussian at this time,

$$\rho_t(x,t) = \frac{1}{\pi(4t+1)}e^{-x^2/(4t+1)},$$

with a width w at half maximum that is larger than the corresponding Gaussian half width. In our experiment we measure the width of lines as a function of the delay time between writing and reading; therefore, we are interested in the

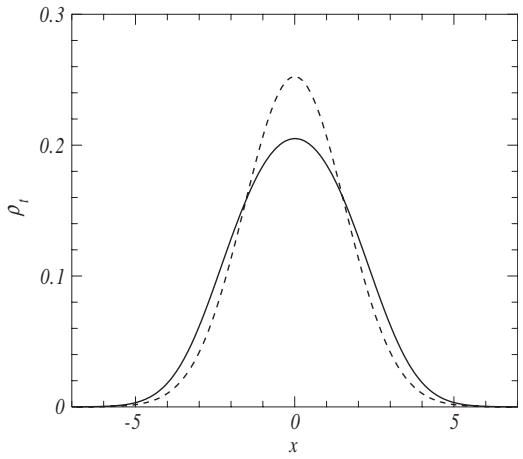

FIG. 7. Solid line: computed line profile at scaled time $t=1$ and scaled initial temperature increase $\Delta T=2$. Dashed line: the corresponding Gaussian profile assuming mass diffusion only.

prediction of our model for the time dependence of w.

Let us recall that for ordinary diffusion $w^2(t)=(4\ln 2)[\sigma^2(0)+4Dt]$, with the factor $(4\ln 2)$ accounting for the ratio between the squared width at half maximum and squared Gaussian width. For the (dimensionless) temperature elevations $\Delta T=0$, 0.4, and 1, the prediction from our model is shown in Fig. 8. It is compared to the nondimensionalized experimental data, with time made dimensionless as $t/[\sigma^2(t_0)/D]$ and normalized squared width $4\ln 2[\sigma^2(t)/\sigma^2(t_0)-1]$, where t_0 is the first measured time delay. The points in Fig. 8, which provide an enlarged view on the anomalous behavior of the squared Gaussian width $\sigma^2(t)$, are the result of a more precise experiment (averages over 800 lines) done in ambient air.

It appears that $\Delta T=0.4$ provides the best fit with the experimental data. Therefore, we learn from this simple model that the initial temperature increase of the spreading line is $0.4\times 273\approx 100$ K. Notice that our prediction is compared to the *growth* of the experimental linewidth since t_0. Any processes before that time are outside the scope of our model.

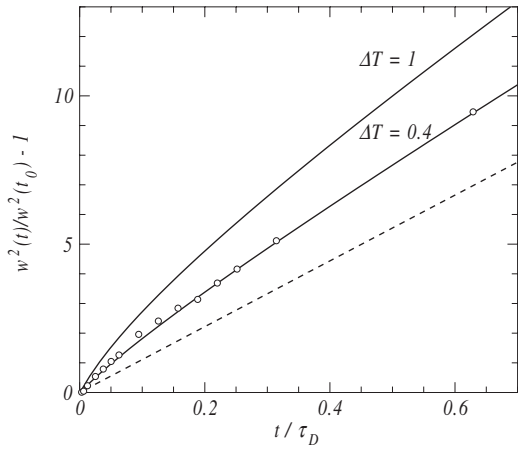

FIG. 8. Solid lines: full width at half maximum $w^2(t)$ computed for initial temperature elevations $\Delta T=0.4, 1$. Dashed line: ordinary diffusion ($\Delta T=0$). Open circles: measured linewidths. The excellent fit of the model to the experiment suggests that the initial temperature increase in the experiment is ≈ 100 K.

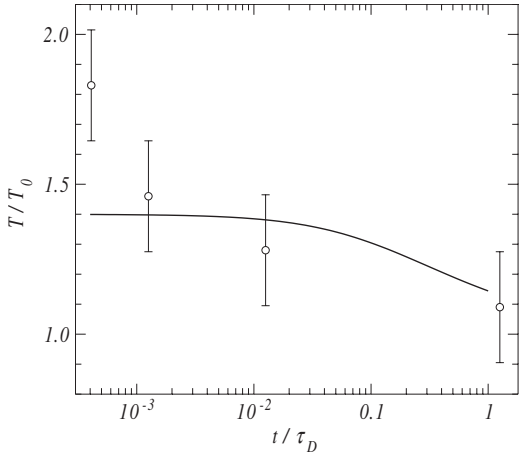

FIG. 9. Solid line: prediction of our convection model with a scaled initial temperature $\Delta T=0.4$ above ambient which produced the best fit in Fig. 8. Open circles: spectroscopically measured temperature. On the dimensionless time scale, the maximum NO concentration is reached at $t/\tau_D\approx 10^{-2}$, while the Kolmogorov time scale is at $\tau_\eta/\tau_D\approx 10^{-1}$.

In our model the temperature decays through heat diffusion and convection. This decay is compared to the time-dependent line temperature that was measured in a separate experiment. In this experiment the camera was zoomed in on a small part of the line around the focus (150 μm $\times$ 150 μm) and an NO excitation spectrum was acquired by scanning the dye laser over a wavelength range of $\lambda=225.45-225.75$ nm. The relative peak intensities in this spectrum depend on the local temperature. The measured spectrum was then compared to the simulation of the excitation spectrum, calculated using LIFBASE which has the temperature as a parameter [21]. Thus, an effective line temperature can be found. These measurements were repeated for several delay times between writing and reading.

Figure 9 shows a rapid initial decay of the measured line temperature. At early times, writing involves complex chemical pathways leading to a maximum NO concentration at $t\approx 2$ μs. During these times, which are much shorter than the Kolmogorov time and which precede the time delay of the first measured point in Fig. 8, all the heat is released. Our model applies to the episode after this one, where the predicted temperature dependence can be compared well to the measured one.

Let us now return to the pressure dependence of the effective diffusion coefficient in Fig. 6. In our model, the role of the pressure is a rescaling of the time axis. Notably, at $p=11$ bars, the dimensionless times in our experiment are an order of magnitude shorter than at atmospheric pressures. At high pressures, therefore, we may pick up the anomalous acceleration of the spreading rate such as shown in Fig. 8. This effect could be aggravated by an increase of the initial temperature rise ΔT for increasing pressures.

If this temperature rise were the same for all pressures, all measured spreading rates $w^2(t)/w^2(t_0)-1$ would collapse when the delay times are scaled with $\tau_D=p\sigma^2(t_0)/D$, with p the relative pressure ($p=1$ at standard conditions). Figure 10 shows that this is not the case.

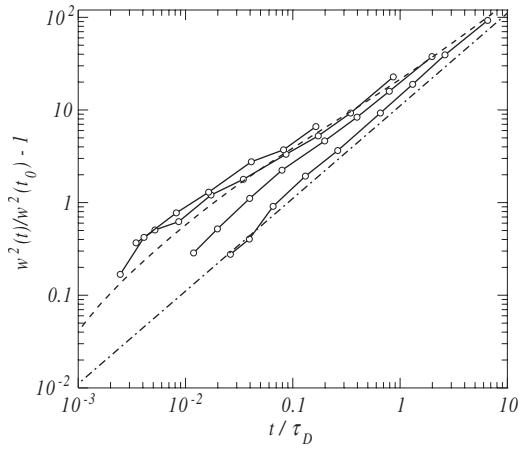

FIG. 10. The data of Fig. 5, but now plotted in dimensionless units. Dots connected by lines: measured spreading rates of written lines at pressures $p=1$, 3, 6, and 11 bars, respectively. The pressure is increasing from the lowest to the highest curve. The experiments were done in an oxygen-poor environment (a mixture of 99.76% N_2 and 0.24% O_2). The time axis is scaled with $\tau_D=p\sigma^2(t_0)/D$. Dashed line: prediction from our model for an initial temperature rise $\Delta T=2$. Dash-dotted line: ordinary molecular diffusion $w^2(t)/w^2(t_0)-1=16\ln 2t/\tau_D$, where a factor 4 ln 2 accounts for the ratio between half width w^2 and Gaussian width σ^2.

We conclude that with increasing pressure also the initial temperature rise ΔT increases. This is illustrated by the result from our model for $\Delta T=2$ which now closely resembles the measured spreading rate at $p=6$ and $p=11$ bars. A possible explanation for this pressure dependence is that the initial temperature rise T_0 is caused by the heat released in chemical reactions whose rates are proportional to the squared density.

Our experiment has (approximate) cylindrical symmetry whereas our model assumes a linear geometry. As can be verified easily, the trick embodied in Eq. (12) fails in cylindrical coordinates and an analytical solution of our model cannot be reached. However, we believe that our conclusions will qualitatively be the same in the cylindrical symmetry.

VI. NONLINEARITY OF THE WRITING PROCESS

The formation of our molecular tags involves a nonlinear photochemical process which has only been identified partly [12]. What is most important for the art of writing is how the written tracer concentration C depends on the intensity I of the writing laser beam. A highly nonlinear response would open up the possibility of writing dots by crossing two laser beams. Specifically, if the concentration C of NO molecules depends on the writing laser intensity I as $C(I)\propto I^D$ and two beams of equal intensity are crossed, the ratio R_I of the NO concentration in the intersection point over that of the sum of the crossing lines would be 2^{D-1}. If the exponent D is large enough, only the intersection point will be seen. This would be the case if writing proceeds through a high-order multiphoton process.

We performed two experiments in still air to assess the nonlinearity of the writing process. In the first one we split the writing beam in two parts, focused each of them, and crossed them at right angles in their respective foci (see Fig. 2). We then used the shot-to-shot intensity variation of the writing laser to scan the response function $C(I)$. The NO molecules were visualized by inducing fluorescence 3 μs after writing. For each laser shot we analyzed the registered fluorescence image by fitting Gaussians to the cross sections of the intersecting beams, $I(z)=I_0+I\exp(-z^2/\sigma^2)$, with the line center at $z=0$. This provided the intensities I_1 and I_2 of the intersecting beams and the intensity I_s of the intersection point [see Fig. 11(a)]. Because the maximum registered intensity of the 12-bit camera has pixel value 4095, the ratio of the intensities is limited by $4095/(I_1+I_2)$. We have performed two experiments, both with 10^3 images of crossing lines, but with one at a reduced laser power. The result is shown in Fig. 11(b).

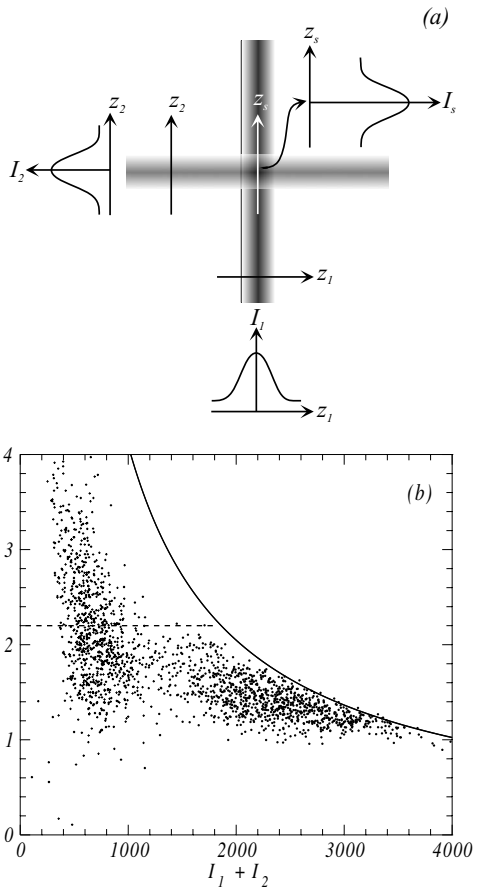

FIG. 11. Measuring the nonlinearity of the writing process by intersecting two writing beams. (a) The intensities are measured in the image by fitting Gaussians to the shown cross sections. (b) Dots: ratio $R_I=I_s/(I_1+I_2)$ for 10^3 laser shots. Solid line: limit $4095/(I_1+I_2)$ set by the 12-bit camera used. In fact, the intensity I_1 is an average over the cross sections left (shown) and right of the intersection, and analogously for I_2. Two data sets are shown, one with a mean intensity $\langle I_1+I_2\rangle=700$, the other one with $\langle I_1+I_2\rangle=2300$. Dashed line: mean R_I of the second data set.

For each of the data sets, the laser intensity has ≈30% shot-to-shot variation. We find that the writing nonlinearity is approximately 2. However, since it is difficult to perfectly overlap the writing beams (which have a Gaussian width $\sigma\approx 50$ μm), the measured nonlinearity may have been under-

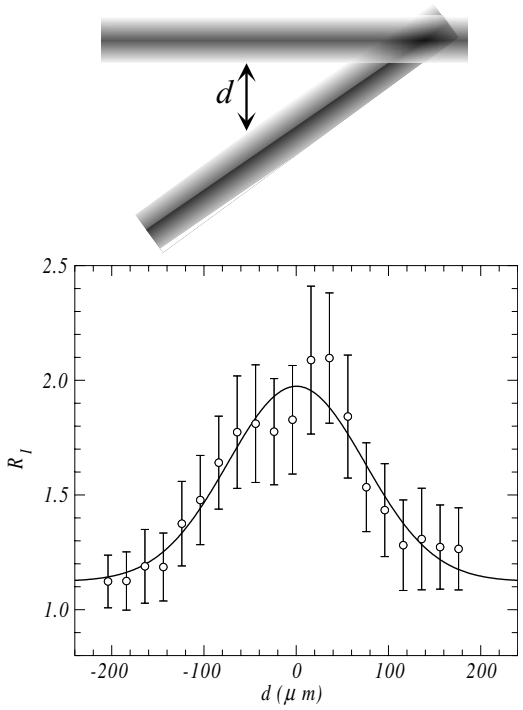

FIG. 12. Measuring the nonlinearity of the writing process by moving two writing beams through their intersection point. Open circles: ratio $R_I=I_s/(I_1+I_2)$ for 100 laser shots each; the size of the error bars indicates the rms fluctuation. Solid line: Gaussian fit $R_I(d)\sim\exp[-(d/\sigma_s)^2]$, with $\sigma_s=100$ μm.

estimated. Therefore, a second experiment was performed in which the minimum distance d between the two writing beams was adjusted in small (20 μm) steps through the intersection point $d=0$.

The result of this experiment is shown in Fig. 12. At the point of perfect crossing $d=0$, the intensity I_s at the intersection point is twice the sum intensity I_1+I_2 of the crossing beams, which implies that the nonlinearity is quadratic, $D=2$. For such a nonlinearity, the profile $I_s(d)$ is again a Gaussian with width $\sigma_s=(\sigma_1^2+\sigma_2^2)^{1/2}$, where σ_1 and σ_2 are the widths of the crossing beams. These widths follow from the measured Gaussian widths of the crossing lines in the images, $\sigma_{m1}=\sigma_1/2^{1/2}$ and $\sigma_{m2}=\sigma_2/2^{1/2}$, with $\sigma_{m1}=38$ μm, $\sigma_{m2}=32$ μm, and $\sigma_s=70$ μm. The difference with the directly measured $\sigma_s=100$ μm may be explained by the large intensity fluctuations of the laser beams.

The quadratic nonlinearity indicates that the rate-limiting process in the fusion of N_2 and O_2 molecules to NO is a two-photon process with a virtual intermediate quantum state. Several candidate transitions have been identified in a spectroscopic study of our used tagging technique, the results of which will be published elsewhere [12].

It is still possible to use such a modest nonlinearity to write special patterns, such as highlighted intersection points; however, we must realize that in turbulent flows lines develop spontaneous intensity fluctuations due to turbulent mixing. The idea is that the component of the fluctuating velocity directed along the lines concentrates and dilutes the written tracer molecules, resulting in concentration fluctuations along the line. This is illustrated in Fig. 13. Clearly, the

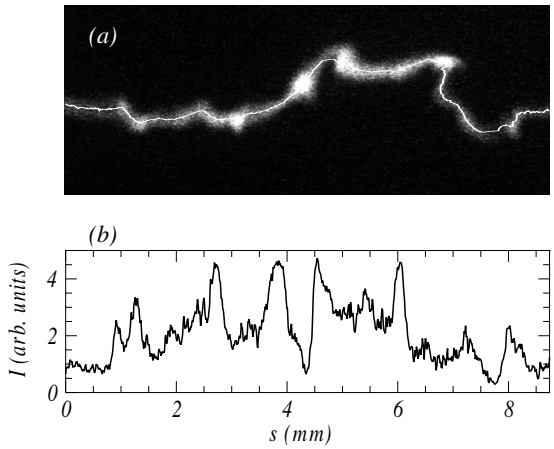

FIG. 13. Spontaneous creation of intensity fluctuations in turbulence. (a) Image of a line of NO molecules in a strongly turbulent jet flow (turbulence Reynolds number $\mathrm{Re}_\lambda=510$). The width of the image is 6.5 mm. The line was imaged 30 μs after it was written and it has developed concentrated clusters of tagged molecules. These clusters are caused by the squeezing and stretching due to the turbulence. The bright line is a fit $\boldsymbol{x}(s)$ to the line center. (b) The line intensity $I(s)$ as a function of the path length s along the line. It was determined by fitting Gaussians to line sections which are oriented perpendicularly to $\boldsymbol{x}(s)$, $I(z,s)=I_0+I(s)\exp(-z^2/\sigma^2)$, where z is the perpendicular coordinate with $z=0$ the line center.

spontaneous clustering of tracers due to turbulence is much larger than what could have been achieved by crossing two beams and exploiting the writing nonlinearity.

VII. CONCLUSION

Due to the role of diffusion, the application of molecular tagging velocimetry to turbulent flows of gases is special. For Sc=1 tracers, the diffusive filter through which turbulent displacements are seen is unavoidable. At small time and length scales, turbulent dispersion is chaotic and particles will separate exponentially in time. Therefore, if two particles start out very close together, it takes a very long time for them to separate. However, for Sc=1 molecules, it only takes one Kolmogorov time for Brownian motion to put them a Kolmogorov length apart. Thus, even if written lines are infinitely thin, they will have broadened to sausages with width η in one small eddy turnover time, after which the content of the sausages is churned by the small-scale eddies, accelerating the line broadening. Therefore, it is the combined action of molecular diffusion and turbulent dispersion that poses a fundamental limit on the resolution of tagging velocimetry. This course of events can only be broken by using molecular tracers with much larger values of the Schmidt number. Several candidate molecules have already been considered in the literature [8,9].

Our tagging scheme has the advantage of stable molecular tags, but the price paid is an increased temperature of the written patterns which enhances their diffusion. However, this anomalous diffusion is still outweighed by the small-scale turbulent dispersion. We have found that the initial temperature rise and the anomalous diffusion increase with

increasing pressure: at 10 bars the line broadening is a factor of 3 faster than given by the molecular diffusion constant. This will affect molecular tagging velocimetry in experiments at large pressure.

The nonlinearity of the pen is important for the art of writing. Since the intensity of the writing laser varies through its focus, a linear dependence of the written tag concentration on the writing laser intensity makes relatively uniform lines. On the other hand, a strongly nonlinear dependence may be used to write dots by crossing two writing beams. In our case, the nonlinearity turns out to be quadratic, which highlights intersections of written lines, but does not turn them into dots. An alternative way to write dots using the quadratic nonlinearity would be to (strongly) focus the laser beam. However, we found it difficult to avoid optical breakdown of the air with focused writing laser beams.

Although molecular tagging velocimetry using molecules with mass comparable to that of air cannot be used to measure the small-scale gradients in a turbulent flow, it offers a unique view on small-scale mixing. By writing patterns in turbulence, scales can be reached which are much smaller than those observable with seeded light scattering particles. The deformation of these patterns provides a microscope on the first stages of turbulent mixing.

ACKNOWLEDGMENTS

We gratefully acknowledge financial support by the Nederlandse Organisatie voor Wetenschappelijk Onderzoek (NWO) and Stichting Fundamenteel Onderzoek der Materie (FOM).

[1] R. B. Miles and W. R. Lempert, Annu. Rev. Fluid Mech. **29**, 285 (1997).
[2] A. Noullez, G. Wallace, W. Lempert, R. B. Miles, and U. Frisch, J. Fluid Mech. **339**, 287 (1997).
[3] R. B. Miles, C. Cohen, J. J. Connors, P. J. Howard, S. Huang, E. C. Markovitz, and G. Russell, Opt. Lett. **12**, 861 (1987).
[4] J. A. Wehrmeyer, L. A. Ribarov, D. A. Oguss, and R. Pitz, Appl. Opt. **38**, 6912 (1999).
[5] R. W. Pitz, J. A. Wehrmeyer, L. A. Ribarov, D. A. Oguss, F. Batliwala, P. A. D. S. Deusch, and P. E. Dimotakis, Meas. Sci. Technol. **11**, 1259 (2000).
[6] L. A. Ribarov, J. A. Wehrmeyer, R. W. Pitz, and R. A. Yetter, Appl. Phys. B: Lasers Opt. **74**, 175 (2002).
[7] R. W. Pitz, M. D. Lahr, Z. W. Douglas, J. A. Wehrmeyer, S. Hu, C. D. Carter, K. Y. Hsu, C. Lum, and M. M. Koochesfahani, Appl. Opt. **44**, 6692 (2005).
[8] B. Hiller, R. A. Booman, C. Hassa, and R. K. Hanson, Rev. Sci. Instrum. **55**, 1964 (1984).
[9] B. Stier and M. M. Koochesfahani, Exp. Fluids **26**, 297 (1999).
[10] N. J. Dam, R. J. H. Klein-Douwel, N. M. Sijtsema, and J. J. ter Meulen, Opt. Lett. **26**, 36 (2001).
[11] W. van de Water, T. Elenbaas, M. Pashtrapanska, J. Bominaar, N. Dam, and J. J. ter Meulen, Exp. Fluids (to be published).
[12] C. Schoemaeckers and N. Dam, Exp. Fluids (to be published).
[13] M. Kass, A. Witkin, and D. Terzopoulos, Int. J. Comput. Vis. **1**, 321 (1988).
[14] C. Xu and J. L. Prince, IEEE Trans. Image Process. **7**, 359 (1998).
[15] P. G. Saffman, J. Fluid Mech. **8**, 273 (1960).
[16] A. Mazzino and M. Vergassola, Europhys. Lett. **37**, 535 (1997).
[17] H. Tennekes and J. L. Lumley, *A First Course in Turbulence* (MIT Press, Boston, 1972).
[18] A. La Porta, G. A. Voth, A. M. Crawford, J. Alexander, and E. Bodenschatz, Nature (London) **409**, 1017 (2001).
[19] A. J. F. Gielen, Ph.D. thesis, Eindhoven University of Technology, 2003.
[20] A. Majda, *Compressible Fluid Flows and Systems of Conservation Laws in Several Space Variables*, Vol. 53 of Applied Mathematical Sciences (Springer, New York, 1984).
[21] J. Luque and D. R. Crosley (unpublished).